Influence of gas sparging on membrane performance

By

Sandra Farran-Lee

Department of Chemical Engineering
Lund University

June 2015

Supervisor: Professor Ann-Sofi Jönsson
Co-supervisor: PhD Johan Thuvander
Examiner: Ass. professor Mattias Alveteg

Postal address	**Visiting address**	**Telephone**
P.O. Box 124	Getingevägen 60	+46 46-222 82 85
SE-221 00 Lund, Sweden		+46 46-222 00 00
Web address		**Telefax**
www.chemeng.lth.se		+46 46-222 45 26

Preface

This master thesis has been performed at the Department of Chemical Engineering at the Faculty of Engineering, LTH, Lund University.

For this project was Ann-Sofi Jönsson from the Department of Chemical Engineering supervisor. I would like to thank her for the advice, suggestions and time she has given me.

The experimental work could not have been conducted without the help, expertise and support from Johan Thuvander. Thanks to Leif Stanley for all help with the technical equipment, that at times seemed to have something against me.

I also would like to thank Xylophane for providing me with the hemicellulose solution used during the experiments.

Sandra Farran-Lee

Lund, June 2015

Abstract

A new oxygen barrier film that is made of arabinoxylan has been developed by the company Xylophane. Arabinoxylan is available among other things in wheat bran. But a problem with the method of extracting the arabinoxylan is that after an alkali extraction is ultrafiltration used to remove impurities and the flux during this is quite low. In this project is it investigated if gas sparging with air can improve the flux for the ultrafiltration step. But first is a study of how gas sparging a silica sol solution affects the flux made. Because silica sol has a similar density and viscosity as the alkali extraction solution from wheat bran. Two different membrane modules were used: a polymeric tubular membrane in the experiments with silica, and a ceramic tubular membrane when treating the hemicellulose solution. The influence of air/liquid ratio, pressure and temperature was investigated.

For the silica sol study the result was that the flux improved when the liquid flow was sparged with air. The studied air flow interval did not reach the point where the flux increase levelled off or decreased. Therefore, a higher flux can be expected when using a higher air flow than the ones studied. The optimal transmembrane pressure (TMP) for the two examined concentrations of silica were 1 bar for the low concentration and 0.6 bar for the higher.

When the hemicellulose solution was studied air was added into the feed tank by letting the retentate flow whip the liquid surface in the feed tank, instead of directly adding it to the liquid flow as in the silica experiments. Hence the amount of air added could not be measured, but the effect it had when the temperature of the solution was 80 °C was substantial. A flux increase over 200 % was reached and if the air addition was terminated, the flux still remained the same. When the temperature instead was 30 °C there was no increase in flux accompanied with the air addition. After performing several analyses on the samples taken from the start of and during, the air addition it was it clear that a degradation of molecules had occurred at 80 °C, but not at 30 °C. This degradation can contribute to the increase in flux, but if it is the only factor can not be determined.

No examination was made regarding the effect the heat and addition of air on the arabinoxylan. Such effects need to be examined before the method can by recommended for the industry this must be examined.

Sammanfattning

En ny syrebarriärfilm som är gjord av arabinoxylan har utvecklats av företaget Xylophane. Arabinoxylan finns bland annat i vetekli. Ett problem med metoden som används för att extrahera det är att efter en alkaliextraktion används ultrafiltrering för att ta bort orenheter och fluxet under ultrafilteringen är ganska lågt. I detta projekt undersöktes om luftning kan förbättra fluxet för ultrafiltrationssteget. Först gjordes en studie av hur luftning påverkar en kiseldioxidsollösnings flux. Denna lösning har en liknande densitet och viskositet som alkaliextraktionslösningen från vetekli. Två olika membranmoduler har använts: ett polymerttubmembran i experimenten med kisel, och ett keramiskttubmembran när hemicellulosalösningen användes. Inverkan av luft-/vätskeflödet, trycket och temperaturen undersöktes.

För studien med kiseldioxidsol var resultatet att fluxet förbättrades när vätskeflödet injeserades med luft. För det studerade luftflödetsintervallet var inte punkten där fluxökningen planade ut eller minskade nådd. Därmed kan det antas att högre flux kan fås med högre luftflöden än de som studerades. Det optimala transmembrantrycket (TMP) för de två undersökta koncentrationerna av kisel var 1 bar för den låga koncentrationen och 0.6 bar för den högre.

När hemicellulosalösningen studerades tillsattes luft till matartanken genom att låta retentatflödet slå ned i vätskan, istället för att tillsätta det direkt till vätskeflödet som vid kisel sol experimenten. Därför kan inte mängden tillsatt luft mätas, men effekten den har när temperaturen på lösningen var 80 °C var stor. En fluxökning på över 200 % nåddes och när tillsättningen av luft avbröts genom att sänka ned retentatledningen under vätskeytan i feedtanken bibehölls fluxnivån. Vid 30 °C istället var där ingen ökning av fluxet med lufttillsättning. Efter att ett antal analyser av prov tagna från och med starten av lufttillsättning och under den gjorts var det klart att en nedbrytning av molekyler hade skett vid 80 °C, men inte vid 30 °C. Denna nedbrytning bidrar definitivt till fluxökningen, men om det är den ända faktorn har inte kunnat avgöras i detta arbete.

Ingen undersökning om arabinoxylanen påverkades av värmen och lufttillsättningen gjordes. Sådana effekter behöver undersökas innan metoden kan rekommenderas till industrin måste detta undersökas.

Table of Contents

1 Introduction

Today, the world is heavily dependent on fossil resources. It is therefore important to find new feedstocks to replace fossil raw materials. Ethylene vinyl alcohol is a material of fossil origin, used as oxygen barrier in food packaging. Barrier films could just as well be manufactured from arabinoxylan recovered from wheat bran, and other hemicelluloses extracted from lignocellulosic materials. Wheat bran is a potential feedstock that is cheap and available in sufficiently large quantities. (Krawczyk, et al., 2011)

An extraction method that provides high yields of arabinoxylan, without significant damage of the polymeric structure, from wheat bran is alkali extraction. For the removal of impurities from the extraction solution ultrafiltration can be used. The only problem with ultrafiltration in this case is that the flux is relatively low, due to the high viscosity and the formation of a gel layer on the membrane surface. Several ways to lower the viscosity of the solution has been tried, like heat treatment, dead-end filtration with kieselguhr and centrifugation with varying result. (Thuvander, et al., 2014) (Krawczyk, et al., 2013)

Gas sparging is a method that has been found to increase flux. In this method a gas is added to the liquid stream to create a gas-liquid two-phase flow. The increased hydrodynamic instabilities caused by the addition of gas increase the shearing forces and lowers the formation of gel layers on the membrane surface. (Cheng & Wu, 2003)

The aim of this work was to study the influence of gas sparging on flux during ultrafiltration of a two different solutions: a silica sol and a hemicellulose-rich solution extracted from wheat bran. Two different membrane modules were used: a polymeric tubular membrane in the experiments with silica, and a ceramic tubular membrane when treating the hemicellulose solution. The influence of air/liquid ratio, pressure and temperature was investigated.

2 Literature Review

2.1 Membranes processes

One of the main problems that chemical industries are faced with is the separation, concentration and purification of molecular mixtures. Effective separation methods are also needed for water treatment and in food and pharmaceutical industries. The common way to deal with this at the moment is to use a number of different techniques, like distillation, adsorption, sedimentation etc. But the relatively new technique of using membranes to solve many of these problems is growing in popularity. The reason for this is that membrane processes are often more energy efficient, simpler to operate and yield higher quality products then other processes. Another bonus with membrane processes are that they are more environmentally friendly, since no hazardous chemicals are used and there is no heat generation. (Strathmann, 2011)

In membrane processes pressure and specially designed synthetic and semi-permeable membranes is used to separate particles on the basis of their molecular size and shape. Membranes are generally built with two layers, a porous support and a thin dense top layer that is the real membrane. The streams that pass through and are retained are called permeate and retentate respectively, as shown in Figure 2.1. (Calabrò & Basile, 2011)

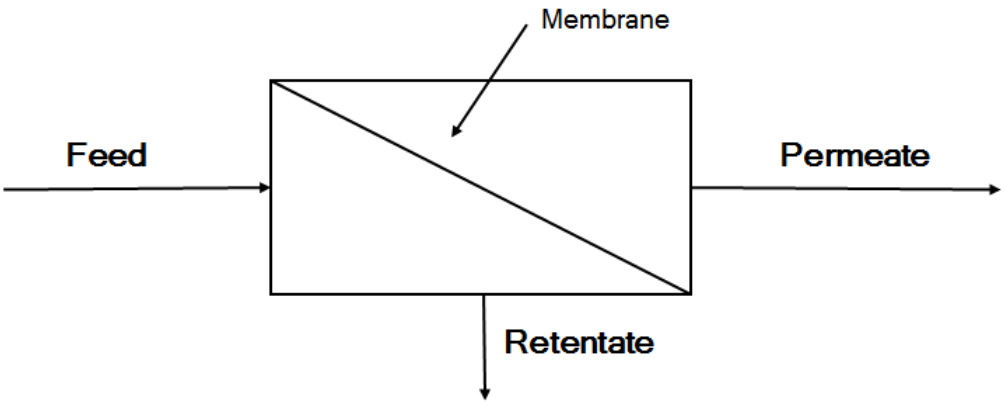

Figure 2.1. Process streams in a membrane module.

Membranes retention ability depends on the pore size, which can vary between 0.1 - 5000 nm. Depending on the size of the smallest particles removed by a membrane or filter are they divided into different groups, see Table 2.1. (Calabrò & Basile, 2011)

Table 2.1. The different processes for membrane separation and the size of the smallest particles they can remove.

Process for membrane separation	Smallest particle size removed
Particle filtration	1 µm
Microfiltration	50 nm
Ultrafiltration	3 nm
Nanofiltration	1 nm
Reverse osmosis	0.1 nm

A large diversity of synthetic membranes exist, since their physical structure and the materials they are made from can differ. Examples of materials that are used for membranes are polymers, ceramics, glass, metals and liquids. (Strathmann, 2011)

The particle size of the two molecules that are to be concentrated in this project leads to that ultrafiltration is the best membrane separation process in this case. Therefore only ultrafiltration shortly is presented.

2.1.1 Ultrafiltration

Ultrafiltration is used when macromolecules, colloids, proteins etc. are to be separated from smaller particles like water and salts. The driving force for the separation over the membrane is the pressure difference over it, as shown in Figure 2.2. It is called the transmembrane pressure (TMP) and for ultrafiltration is its value between 0.1 – 1 MPa. (Jönsson, u.d.)

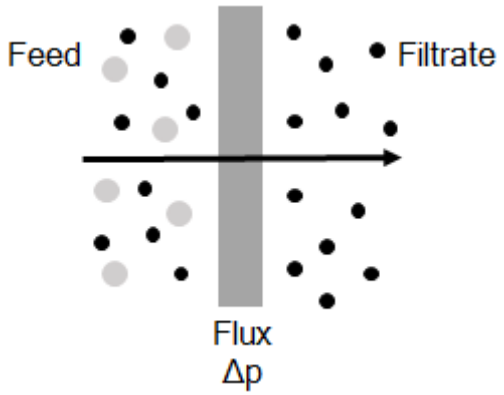

Figure 2.2. Schematic illustrating of the principle of ultrafiltration.

The two methods dead-end and cross-flow filtration is used for ultrafiltration. During dead-end the feed solution is forced under pressure straight through the membrane. An accumulation of the rejected particles forms on the membrane surface and to maintain a constant flow an increase in pressure is needed. In the end the membrane will be so blocked by particles that it must be replaced. During cross-flow filtration the feed solution is flowing along the membrane surface. Larger particles are retained while small ones pass through the membrane and forms a particle-free permeate. Compared to dead-end filtration the equipment needed for cross-flow filtration is more complex, but the flux rates and membrane lifetime are much better. (Cassano & Basile, 2011)

2.2 Gas sparging

A common problem in ultrafiltration and microfiltration is that solutes, which do not pass through the membrane, can accumulate near the membrane surface. This phenomenon is called concentration polarization. If the concentration at the membrane becomes sufficiently high, a cake layer can form on the membrane surface. The filtration resistance becomes higher because of concentration polarization and the cake. This results in a lower flux through the membrane. A way to lower the impact of these two phenomena is to use the method gas sparging. In this method a gas is added to the liquid stream to create a gas-liquid two-phase flow. The increased hydrodynamic instabilities the addition of gas causes, lowers the accumulation of solutes near the membrane, and fouling. (Cheng & Wu, 2003)

2.2.1 Two-phase flow patterns

The size and spatial distribution of the bubbles determines the flow instability and gas-liquid exchange process. Another thing that determines the efficiency of the two-phase flow is the flow pattern. When the flow contains dissolved particles, the effect of dissolved surface-active agents on bubble shape, size and mobility needs to be considered. The last thing that must be considered is the physical effects, such as inertia, capillary forces or shear for the boundary between the gas and liquid. (Wibisono, et al., 2013)

The flow pattern in two-phase flow depends on several parameters:

- The volume fraction of gas and liquid
- The velocity differences between the phases
- The fluid properties
- Slip velocity (the velocity of the gas phase relative to that of the liquid phase)

There are two operational modes for the flowing gas/liquid in membrane processes. They are co-current flow, where gas and liquid flows in the same direction, and counter-current flow, where gas flow in the opposite direction as the liquid flow. Co-current flow is used for air sparging in flat-sheet, tubular, and spiral-wound modules, and for aeration in membrane bio-

reactors. Counter-current flow is used for membrane distillation and membrane contactors. (Wibisono, et al., 2013)

Tubular membranes are usually oriented vertical or horizontal. The orientation and the kind of flow (down-flow or up-flow) influence the liquids hydrodynamics. Therefore are there some differences in the flow patterns for vertical or horizontal oriented tubes. It is more difficult to predict the flow pattern for horizontal tubes than for vertical tubes. Stratified flow (see Figure 2.4) is very common in horizontal tubes, due to differences in density that cause the phases to split up with the heavier liquid phase at the bottom of the tube. For tubes that are inclined on other angles than vertical and horizontal a form of slug flow is very common. Stratification is then hindered by the effect of gravity on the liquid. (Ghajar, 2005)

For co-current vertical upward tubular channels the following flow patterns, with increasing amount of gas, are seen. (Wibisono, et al., 2013)

- Bubble flow: The gas phase appears as small bubbles evenly distributed in a continuous liquid phase, with some tendency to concentrate toward the center of the tube.
- Plug flow: In this flow pattern the gas phase form scattered plugs or pistons with defined phase boundaries, sometimes designated as Taylor bubbles. Taylor bubbles are separated by slugs of continuous liquid which bridge the tube and contain small gas bubbles.
- Slug flow: Is similar to plug flow, but the gas phase is larger bullet-shaped bubbles with less clear phase boundaries.
- Churn flow: In this flow pattern becomes the bullet-shaped Taylor bubbles becomes narrow and distort, which makes it a more chaotic, frothy and discorded than slug flow. The continuity of the liquid in the slug between successive Taylor bubbles is repeatedly destroyed by a high local gas concentration in the slug.
- Annular flow: The gas phase occupies the center of the tube and the liquid phase moves along the tube walls. Some droplets or small bubbles can be located in the gas phase.

For the co-current horizontal tubular channels the following flow patterns, with increasing amount of gas, are seen. (Wibisono, et al., 2013)

- Stratified smooth flow: The gas and liquid flow rates are quite low. The liquid flowing along the bottom of the tube, while the gas is flowing over a smooth liquid/gas interface.
- Stratified wavy flow: The flow pattern is very similar to stratified smooth flow, but the increase in the gas flow rate makes the liquid/gas interface rippled or wavy.

- Bubble flow: At high ratios of liquid flow rate to gas flow rate this pattern is widespread. The gas travels at a velocity similar to liquid in form of small bubbles that tend to concentrate near the top of the tube at lower liquid velocities.
- Plug flow: Along the upper part of the tube moves gas and liquid plugs alternate.
- Slug flow: Quite similar to plug flow, but here are alternate large bullet-shaped gas bubbles that move along the upper part of the tube. Severe vibrations in the tube can occur.
- Annular flow: The gas flows in the center of the tube and the liquid along the tube walls. Some liquid can occur as droplets in the gas center.

Models of fully-developed flow patterns for tubular channels in co-current mode are shown in Figure 2.3 (vertical upward flow) and Figure 2.4 (horizontal flow). The flow patterns are presented as a function of liquid velocity (u_L) and gas/liquid ratio $\theta = (u_G/u_L+u_G)$. The main difference between the two figures is that for the horizontal orientated tubes are the flow stratified. Otherwise the same flow patterns are roughly occurring.

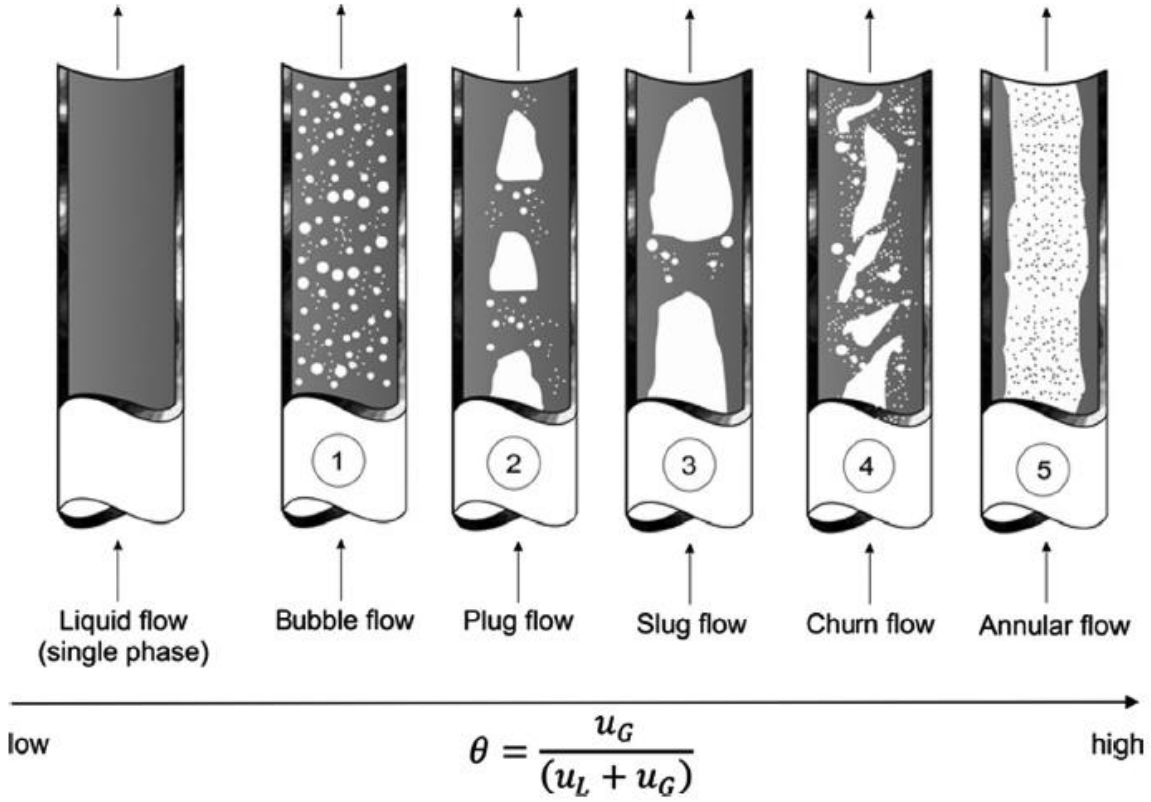

Figure 2.3. Models of basic flow patterns in co-current vertical upward tubular channels. (Wibisono, et al., 2013) Reproduced with permission from Elsevier, September 2015.

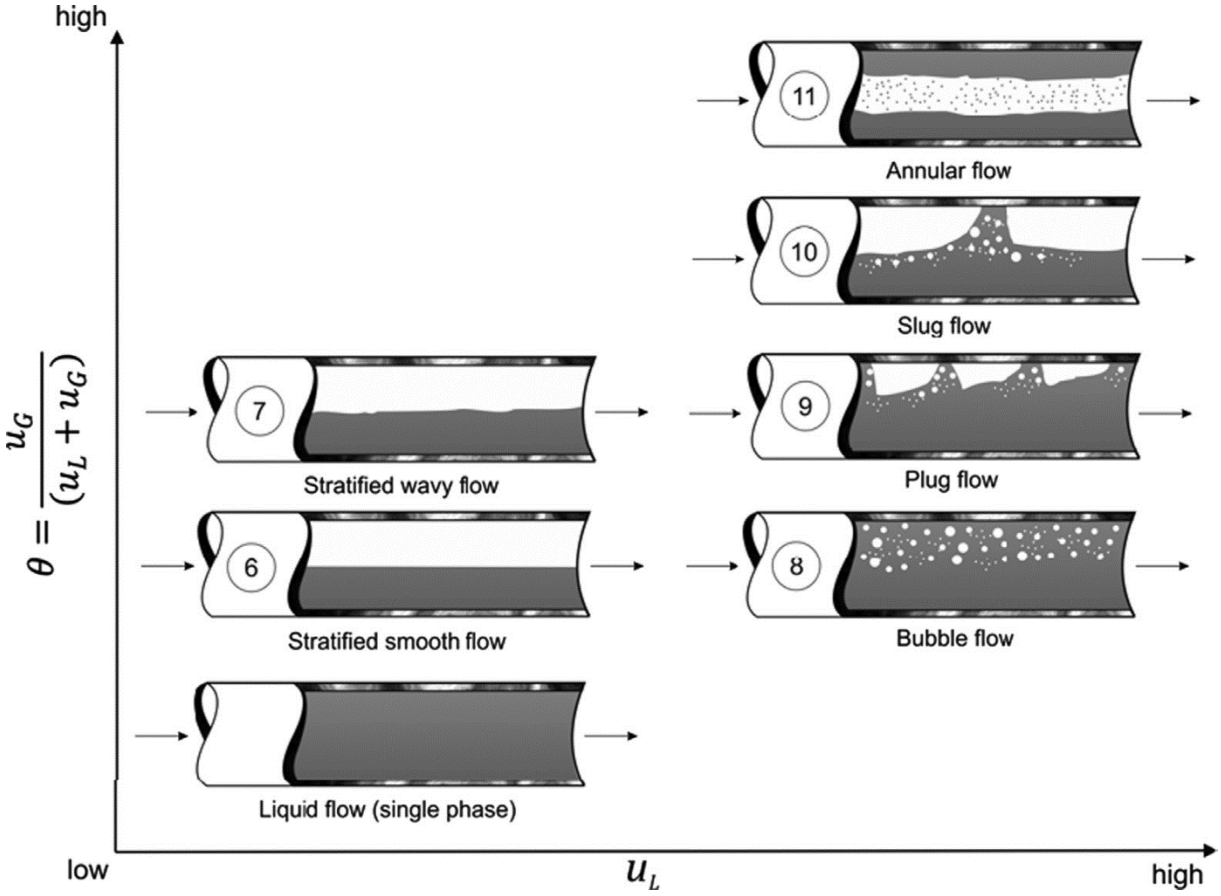

Figure 2.4. Models of basic flow patterns in co-current horizontal tubular channels. (Wibisono, et al., 2013) Reproduced with permission from Elsevier, September 2015.

It is the hydrodynamic forces that determine the bubble shape, along with bubble size and distribution. Slug bubbles are more effective than dispersed bubbles to increase the wall shear stress. That means that slug flow removes more of the solute build up near and on the membrane. For submerged membranes bubble flow is instead more efficient. The ratio between gas/liquid flow must be constant to maintain the chosen flow pattern, since they are related. (Wibisono, et al., 2013)

Flux improvements with gas sparging have been seen for both upwards and downwards flow using vertical tubes. For bubble flow, i.e. low gas and liquid velocities, the increase in flux between upward and downward flow is quite the same. But for slug flow, i.e. high gas velocities, downward flow give higher fluxes than upward flow. The difference in the two flows hydrodynamics are what is causing that. This difference should result in a polarization layer that is thinner for the downward flow and therefore gives a higher flux enhancement. (Cabassud, et al., 2001)

2.2.2 Influence of particles in feed

Unfortunately the flow pattern of liquids containing solutes differs from that of clean water. Solutes and particles in the liquid lead to a decrease of interfacial energy and interfacial tension. Another effect of the presence of solutes is that the bubble interface can become deformed. (Wibisono, et al., 2013)

Figure 2.5 shows how impurities in a stagnant liquid affect a small bubble rising through it. Solutes and particles in the liquids are moved by the shear forces to the wake region of the bubble. This can slow down or even stop the bubble, since a gradient of surface tension (σ) occurs that's goes against the motion of the interface. In liquids with impurities do bubbles with small diameters act as rigid spheres when they are rising. Depending on how much impurities the liquid is containing, the bubbles with large diameters will form wobbling ellipsoidal shapes or spherical caps. (Wibisono, et al., 2013)

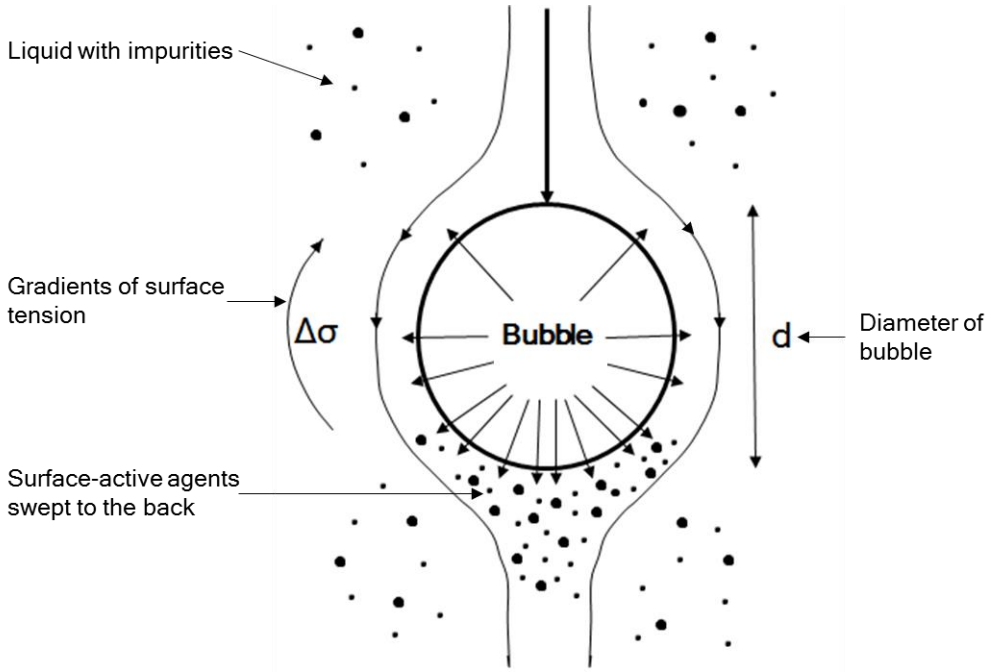

Figure 2.5. Interface of rigid bubble formed by surface impurities. Adopted from (Wibisono, et al., 2013).

2.2.3 Flotation

If a particle is hydrophobic it can become attached to a gas bubble. This occurs when the particle and bubble are adequately close. The particles approach to the bubbles is controlled by the hydrodynamics in the liquid they are immersed in. It is the range of the attractive surface forces that decides how close the particle must come to the bubble to be captured. When a particle comes close enough to be captured, the liquid film between the particle and the bubble starts to diminish. When the critical thickness of the liquid film is reached, it will rupture.

This results in a movement of the boundary between the surface of the solid particle, receding liquid phase and advancing gas phase, so that a stable wetting perimeter is formed. The stable particle-bubble aggregate can only by broken when the kinetic energy is greater or equal to the detachment energy. (Ralston, et al., 1999)

2.3 Recovery of hemicelluloses from wheat bran

The reason that arabinoxylan and other hemicelluloses in lignocellulosic materials are an interest of research are the properties it has as a feedstock for the manufacture of products, such as oxygen barrier films for food packaging materials. Oxygen barrier films today are made from ethylene vinyl alcohol that has a fossil source origin. (Krawczyk, et al., 2011) A number of different methods to extract arabinoxylan from agricultural residues, like wheat bran, have therefore been developed (Krawczyk, et al., 2013). Alkali extraction and hot water extraction are two of these methods. Extraction with alkali have given high yield and low polymer degradation. Since more components than arabinoxylan remains after the extraction are further purification needed. (Thuvander, et al., 2014)

Precipitation with ethanol, ultrafiltration and chromatography are three common purification methods for hemicelluloses extracted from lignocellulosic materials. Even if more homogeneous fractions are attained with ethanol precipitation and chromatography, is ultrafiltration a good option since it has low chemical consumption and low energy requirement. (Arkell, et al., 2013)

Due to the fact that wheat bran is available in suitably large quantities gives it a high potential as a material source for arabinoxylan. A problem is that after the alkali extraction are the high viscosity of the solution, due to the content of high-molecular mass substances. In tubular membranes this can lead to high frictional pressure drops along the membrane during ultrafiltration. This results in a lower flux of the membrane. (Krawczyk, et al., 2011)

Several studies of how the pressure drop over the membrane can be reduced or eliminated have been performed. In all this studies is a tubular ceramic membrane made of α-Al_2O_3 with TiO_2 top layer and the sealing material on the end caps of the membrane was polytetrafluoroethylene used.

The operating parameters TMP, temperature, cross-flow velocity and solution concentration were varied in order to establish optimal conditions for ultrafiltration of a hemicellulose solution (Krawczyk, et al., 2011). The result was that the operating parameters affected the flux significantly, but had no influence on the retention of the membrane. A decrease in the apparent viscosity contributed mostly to the flux increase. At the low TMP of 0.8 bar was the limiting flux reached even with a high temperature and high cross-flow. A lower feed concentration leads to higher flux.

It has been investigated if two pre-filtration methods, microfiltration and dead-end filtration with kieselguhr, could remove the gelforming substances and therefore decrease the viscosity of the arabinoxylan solution (Krawczyk, et al., 2013). Under various operating condition was then the changes on the flux and retention measured. Both pre-filtration methods lowered the viscosity and much higher fluxes were reached during ultrafiltration. The yield of arabinoxylan was much less when microfiltration was performed before ultrafiltration. That was not the case with dead-end filtration, less than 5% of the hemicelluloses were lost. A threefold increase of the flux during ultrafiltration was achieved when dead-end filtration with kieselguhr was used as the pre-filtration method.

In an investigation (Arkell, et al., 2013) it was analysed if it is the viscosity or suspended matter that influences the flux the most. This was done by subject the solution to heat treatment and there by decrease the viscosity of the solution. It was found that the flux increased 1.3 times if the hemicellulose extraction were heat treated for three days at 80 °C. The conclusion that a heat-insensitive substance affected the solutions viscosity was drawn.

If centrifugation can remove suspended solids from the extracted hemicellulose solution were investigated (Thuvander, et al., 2014). Three pretreatment methods for ultrafiltration was studied: increasing the residence time in the nozzle separator already used for pretreatment of the hemicellulose solution, removing dense components using high-speed centrifugation, and centrifugation prior to dead-end filtration with kieselguhr in order to lower the filter cake resistance during dead-end filtration. It was found that centrifugation did lower the turbidity and viscosity for the solution. But with centrifugation alone was not the flux during ultrafiltration increased in a considerable way. The turbidity and viscosity of the solution was reduced much by dead-end filtration. The flux during ultrafiltration was twice as high when it was pretreated with dead-end filtration compared to untreated. When both centrifugation and dead-end filtration with kieselguhr were used as pretreatment was the flux during ultrafiltration almost three times higher.

3 Materials and method

3.1 Silica sol experiment

3.1.1 Solutions

The silica sol solution used in the experiments was Bindzil 30/220 from AkzoNobel. It had a concentration of 30 %, so it were diluted with deionized water to get the two different concentrations of 0.5 % and 5 % and the final volume of at least 40 L.

3.1.2 Equipment

Membrane

A polymeric membrane made of polyvinyldifluoride (PVDF) was used in the silica sol experiments. In Table 3.1 are the specifications of the membrane given. The membrane was position horizontal during the experiments, due to practicality.

Table 3.1. Characteristics of the polymeric membrane used in the silica sol experiments.

Membrane length	1000 mm
Inner diameter	12.7 mm
Number of channels	1
Membrane area	0.0399 m^2
Molecular weight cut-off	200 000 MW

Experimental set-up

In Figure 3.1 is the set-up for the silica sol experiments shown. The tank size was about 100 L and had a removable lid. The polymeric membrane was placed in a membrane housing (diameter 0.5 inches, length 1 m). To control the feed flow was a piston pump (Hydra-cell, D25XL, Wanner) controlled by a frequency converter (ELEX4000, Bergkvist & Co AB, Gothenburg, Sweden) used. The transmembrane pressure (TMP) was adjusted manually with a valve on the retentate side of the membrane.

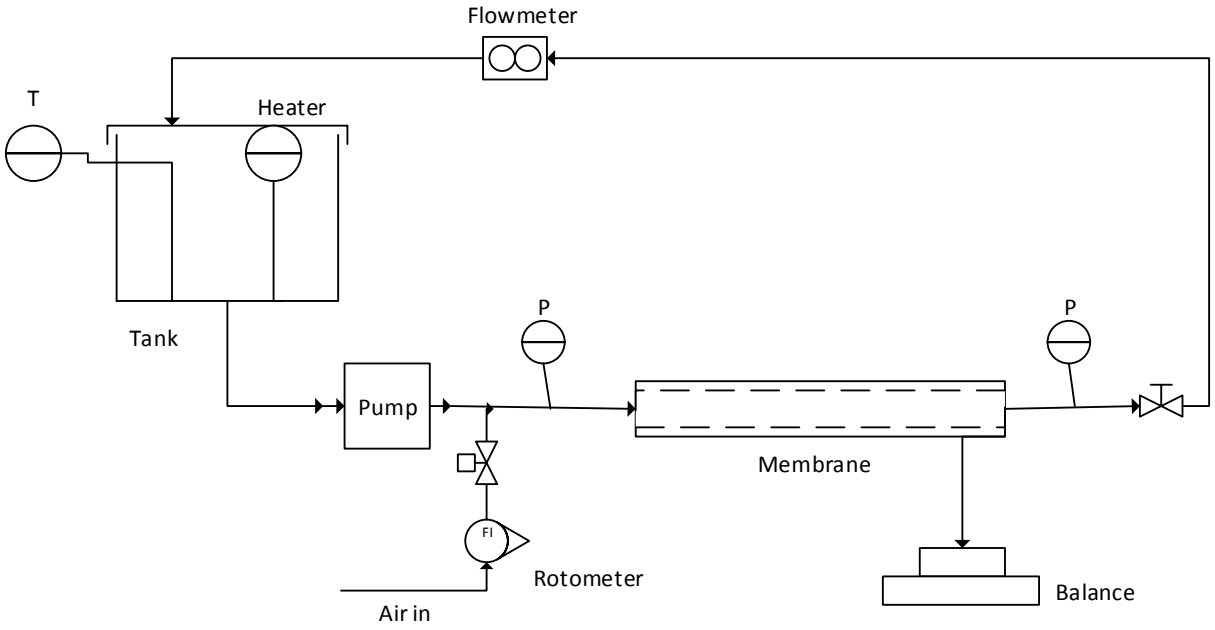

Figure 3.1. Schematic of set-up used in the experiments with silica sol. P: pressure transmitters, T: temperature sensor.

Instrumentation

The temperature of the fluid was controlled with an immersion heater that was coupled with a temperature controller (Shinko MCM, Shinko Europe BV), monitored using two Pt-100 temperature probes (Pentronic) submerged in the feed tank. The pressures in and out of the membrane were measured with two pressure transmitters (Trafag DCS40.0AR, Regal Components AB, Uppsala, Sweden). A flowmeter (Vortex flowmeter, Danfoss, VOR 1100/2000, 380834-004) and a rotometer (Fischer&Porter Co., Ltd.) were used to measure the liquid flow downstream from the membrane and the air flow before entering the system. The permeate flux was measured gravimetrically with an electronic balance (PL6001-L, Mettler-Toledo Inc.). Data were recorded through the measurement devices to a computer using LabView 2009 software (National Instruments Co, Austin, TX, USA).

3.1.3 Experimental procedure

The new membrane was cleaned with a 0.5 wt% solution of an alkaline cleaning agent (Ultrasil 10, Ecolab AB, Älvsjö, Sweden) for 1 h at the temperature of 50 °C and the TMP 0.5 bar before the experiment was performed. After this was the system rinsed twice with deionized water. Then was the pure water flux measured at 30 °C, with the TMP 0.4 to 1 bar with the step size of 0.2.

The temperature was kept constant at 30 °C, and permeate and retentate were returned to the feed tank during the experiments. Three parametric studies each without air for the two differ-

ent concentrations of silica sol, 0.5 % and 5 %, were performed to find out the influence of TMP and cross-flow velocity on the flux. The three cross-flow velocities for this were 1.5, 2 and 2.5 m/s. The studies started with the TMP of 0.4 bar or at the lowest possible pressure achievable, except for the study at 1.5 m/s for 5 % silica sol content where the start value was 0.2 bar. The TMP was then increased stepwise with 0.2 bar until the flux increase levelled off. Running times of 10 minutes for each pressure were performed and measurements for TMP and flux were sampled every 10 s. The average values of the TMP and flux measurements were taken to represent their steady state values.

Parametric studies with air were performed under the same conditions as above. The amount of air added to the liquid flow for 1.5 and 2 m/s were of the volume ratios 1:15.2 and 1:7.6 air/water and the additional of 1 and 2 L/min air for 1.5 m/s. For the liquid flow of 2.5 m/s were only the solution with the concentration of 5 % silica sol air sparged with the ratio 1:15.2 air/water and 2 L/min air. The air flow was adjusted every time the pressure was increased in order to keep a constant air flow throughout the experiments. The liquid flow was measured before the air flow was turned on, because the flowmeter could not measure the liquid flow when air was added to the stream.

3.2 Hemicellulose solution experiment

3.2.1 Solution

Two different batches of an alkali extraction of wheat bran were used in the experiments. One fresh and one already pre-filtered with kieselguhr stored at 4 °C for about two years.

3.2.2 Equipment

Membranes

A tubular ceramic membrane made of a-Al_2O_3 with a TiO_2 top layer was used (Atech Innovations GmbH, Gladbeck, Germany). In Table 3.2 are the specifications of the membrane given. The membrane was vertical during the experiments.

Table 3.2. Characteristics of the ceramic membrane used in the hemicellulose solution experiments.

Membrane length	1000 mm
Outer diameter	25.4 mm
Number of channels	7
Diameter of channels	6 mm
Membrane area	0.132 m^2
Molecular weight cut-off	10 kDa
Sealing material	PTFE

Experimental setup

The system had two 200-L tanks, an M1 module (Atech Innovations) in which the ceramic membrane was installed, and a circulation pump (NB32/25-20, ABS Pump Production, Mölndal, Sweden). In Figure 3.2 is the set-up for the experiment shown. Tank 2 was used as the feed tank during ultrafiltration of the hemicellulose solution and Tank 1 was used for cleaning and start-up. Valves on the permeate and retentate side of the membrane was used to control the transmembrane pressure during ultrafiltration by manually adjusting them. A frequency converter (CDA3000, Lust Antriebstechnik GmbH, Germany) was used to control the pump speed and hence the cross-flow velocity. The transmembrane pressure, TMP, was calculated from the relation:

$$TMP = \frac{P_{in} + P_{out}}{2} - P_p \quad (1)$$

where P_{in}, P_{out} and P_p are the pressures at the inlet, the outlet and on the permeate side of the membrane, respectively. The frictional pressure drop was calculated as the difference between the inlet and outlet pressure.

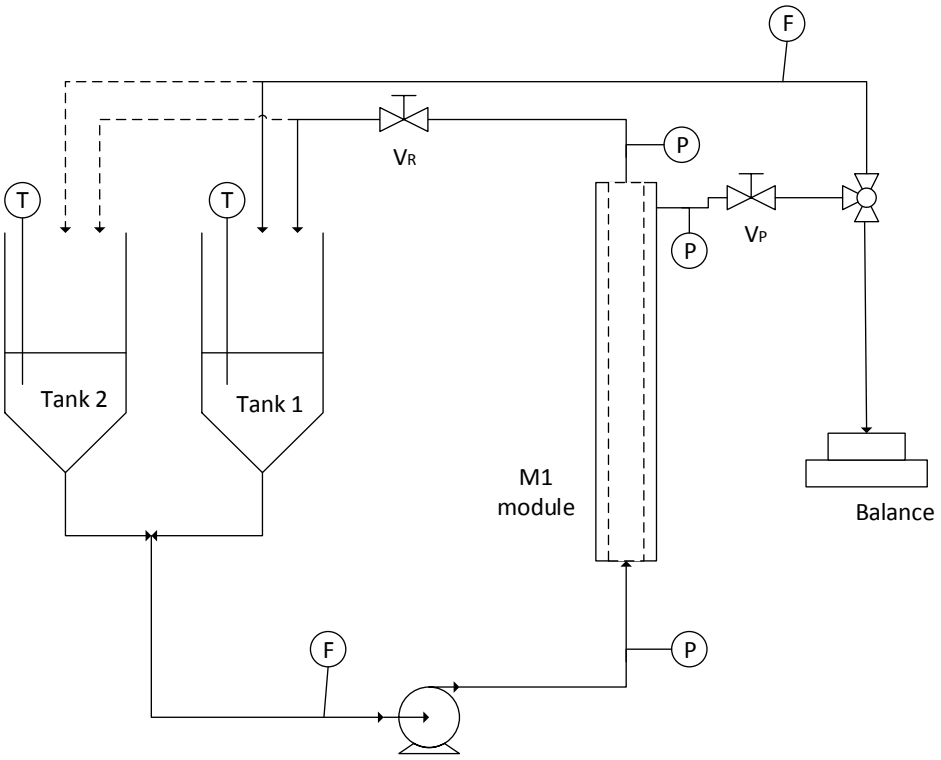

Figure 3.2. Schematic of set-up used in the experiments with the hemicellulose solution. V_R: Retentate valve; V_P: Permeate valve; P: pressure transmitter; T: temperature sensor; F: flowmeter.

Instrumentation

Three pressure transmitters (dTrans p02, Jumo AB, Helsingborg, Sweden) was used in the set-up for the experiment. They were placed at the inlet, the outlet and on the permeate side of the membrane. To measure the feed flow was a volume flow meter (Fischer&Porter Co. Ltd., Göttingen, Germany) used. The permeate flux was measured with a flowmeter (FCH-M-PVDF**,** 92202865, B.I.O-TECH.) or an electronic balance (PL6001-S, Mettler-Toledo Inc., Columbus, OH). In both tanks was a Pt-100 element inserted to measure the temperature. Data were recorded through the measurement devices to a computer using LabView 2009 software (National Instruments Co, Austin, TX, USA).

Filter press

A PF 0.1 H2 filter press (Larox Corp., Lappeenranta, Finland) was used for the dead-end filtration of the solution. A 100 L tank with an agitator, a Pt-100 temperature sensor (Pentronic, Gunnebo, Sweden) and an electrical heater connected to a temperature regulator (Shinko MCM, Shinko Europe BV, Haarsteeg, the Netherlands) for temperature control was used as a preheater vessel. Another 100 L tank equipped with an agitator was used as feed-tank to an air-driven slurry pump (Wilden M2-P Champ, Wilden Pump & Engineering Co., Colton,

CA). The filtration area was 0.1 m^2 and a 10 µm filter cloth (Hydrotech AB, Vellinge, Sweden) was used for filtration.

3.2.3 Experimental procedure

Prefiltration by dead-end filtration

The hemicellulose solution was prefiltrated by dead-end filtration with calcinated and purified kieselguhr (Appli-Chem GmbH, Darmstadt, Germany) to remove large molecules. First were the solution heated under mixing to 50 °C. During this was kieselguhr added to a concentration of 2 wt%. When the desired temperature was reached, the solution was transferred from the heater-tank to the feed-tank. The pressure for filtration was 4 bar. The filtration was performed in batches of the size of 50 or 75 L.

Membrane cleaning

The membrane was cleaned with a 0.5 wt% solution of an alkaline cleaning agent (Ultrasil 11, Ecolab AB, Älvsjö, Sweden) from tank 2 for 1 h at the temperature of 50 °C and the TMP 0.15 bar before and after experimental runs. The crossflow velocity was about 3 m/s. During the cleaning were about 100 L deionized water heated to 50 °C in tank 1. About 60-70 L of this water was used to rinse the system after the cleaning. The rest of the deionized water was circulated in the system and cooled to 30 °C by adding more deionized water. Then was the pure water flux measured with the inlet and outlet pressure of 2.35 and 1.87 bar respectively, a crossflow velocity of about 3 m/s and the TMPs 0.5, 1 and 1.5 bar.

Start-up procedure

To prepare the membrane for the alkali test solution is it pre-treated with an alkali solution with 0.1 M NaOH content. The alkali solution is placed in tank 2 and re-circulated in the system at a crossflow between 2-3 m/s and a sufficiently high TMP until it is time to start an experiment. NaOH solution is heated during circulation to the temperature the hemicellulose solution will have during the experiment. In the meantime is about 80 L hemicellulose solution added to Tank 2 and heated to desired temperature, whilst it is mixed with an external mono pump (SH40R8/C, Mono Pumps Ltd., London, UK). The process solution was used to displace the NaOH solution from the system. The permeate valve was kept closed until the desired crossflow velocity was reach and was the desired TMP gotten by opening it.

Main experiment

During the experiments were permeate and retentate returned to Tank 2. Experiments at the temperatures of 80 and 30 °C were performed. For all experiments but one was fresh solution used and the membrane was cleaned as mention above. To investigate the influence the TMP had on the membrane was the crossflow velocity kept constant on 5 m/s and the TMP was

step wise increased from 0.4 to 1.2 bar with the step size of 0.2 bar. The flux was measured for about 10 min for each investigated TMP.

The TMP was then kept at 1.2 bar for the rest of the experiment time. To investigate how the addition of air affected the flux was the retentate flow pipe raised above the liquid surface in the feed tank when the solution had circulated at the TMP of 1.2 bar for about one hour. For the experiments with fresh solution were feed and permeate samples taken right before and several after the retentate pipe was raised. The experiments was performed for about 4-5 h after that the retentate had been raised. For one experiment was then the retentate pipe then lowered again to investigate if the flux would change. To study if the effect of aeration on flux was reversible was the solution from this experiment kept and a new experiment was made with it the next day. For the other experiments, the hemicellulose solution were displaced from the system with the NaOH solution, heated to the same temperature as the hemicellulose solution, when the experiment was ended. After this was the system cleaned as mentioned above.

3.2.4 Component analysis

Total solids, ash and sodium hydroxide

Total solids is determined by taking 3 ml of each sample to dry in weighed porcelain crucibles with a glass fibre filter at the bottom in an oven at 105 °C for 24 h. After this are the porcelain crucibles put in a desiccator for 30 min before it once again weighed. The weigh difference is the content of total solids.

The dried samples are then put in an oven where they are first heated up to 250 °C and maintained this temperature for 30 min and then to 575 °C for 180 min. After this is the samples cooled to 200 °C in the oven with the door ajar before it is placed in a desiccator to cool for another 30 min and then weighed. The weigh difference is the ash content.

The assumption that the whole ash content was derived from the NaOH from the alkali extraction was made. Since NaOH forms Na_2O and water at high temperatures, see equation 2, must a correction of the weighed be made to decide the NaOH content in the samples.

$$2NaOH \rightarrow Na_2O + H_2O \quad (2)$$

The correction factor 1.29 was used to account for the weight loss of the evaporated water (Krawczyk, et al., 2011).

Acid-insoluble solids and acid-soluble lignin

First were acid hydrolysis performed with about 20 g that is weighed up in hydrolysis bottles and 1.5 ml 72% H_2SO_4 is added. The bottles were placed in an autoclave.

Filter crucibles were taken from the oven at 105 °C and put in a desiccator for 30 min before it was weighed. Then is the fluid from acid hydrolysis vacuum filtered through the filter crucible. The filtrate is put in a container before some deionized water is used to rinse the hydrolysis bottle to get the lignin stock in it. This fluid is then vacuum filtered through the filter crucible. Next is the filter crucibles dried in an oven at 105 °C for 24 h and after being in a desiccator for 30 min is they weighed.

The fluid from the vacuum filtration is used for the analysis for acid-soluble lignin. By measuring the UV absorbance at a wavelength of 320 nm of the fluid in a spectrophotometer is the content of acid-insoluble lignin.

Monomeric sugars

The analysis is performed with the fluid that gone through acid hydrolysis. Before it is diluted a suitable number of times the fluid are filtered through a syringe filter at 0.2 µm. The diluted fluid are transferred to a HPLC-vial and then analyzed in a high-performance anion-exchange chromatography coupled with pulsed amperometric detection. The chromatography system (ICS-3000, Dionex Corp., Sunnyvale, CA) was equipped with a Carbo Pac PA1 analytical column (Dionex Corp.). The used eluent was deionized water at a flow rate of 1 ml/min and a solution of 200 mM NaOH dissolved in 170 mM sodium acetate was used to clean the column. The volume of the sample injection was 10 µl. The sum of the monomeric sugars after anhydro corrections of 0.88 and 0.90 for pentoses and hexoses, respectively, was used to define the concentration of hemicelluloses.

Molecular mass distribution of hemicelluloses and lignin

A Waters 600E chromatography system (Waters, Milford, MA) equipped with a refractive index detector (model 410, Waters) and an UV absorbance detector (model 486, Waters) was used for the size exclusion chromatography to decide the molecular mass distribution of hemicelluloses and lignin. The packing in the analytical column was 30 cm Superdex 30 and 30 cm Superdex 200 (GE Healthcare, Uppsala, Sweden). The used eluent was a 125 mM NaOH solution at a flow rate of 1 ml/min. The calibration of the system was made with polyethylene glycol standards with peak molecular masses of 0.4, 4, 10 and 35 kg/mol (Merck Schuchardt OHG, Hohenbrunn, Germany).

Total lignin

To measure the total lignin content of the samples were they first diluted with deionized water. Then was there UV-absorbance at 280 nm measured with a spectrophotometer (UV-160, Shimadzu Corp., Kyoto, Japan).

4 Results and Discussion

Below are the results from the two experiments presented. For both of them were the pure water flux linear depended on TMP as expected.

4.1 Experiment with silica sol

Ultrafiltration experiments were performed with a silica sol at a concentration of 0.5 wt % and 5 wt %. Just as it was predicted did the flux over the membrane increase when air was added to the silica sol solution stream, as shown in Figure 4.1.

The achieved fluxes in the experiment differ greatly between the two tested silica sol concentrations. In Figure 4.1 b) is the highest flux of 116.5 L/m^2h attained for the lower concentration and higher air flow. The fluxes for the higher concentration are about one third of the ones at the lower concentration. The reason for the difference in flux is likely that a higher particle density at the membrane surface is gotten for the higher concentration. This gives a higher filter resistance and therefore a lower flux.

If the increase in flux between the two concentrations is compared absolutely, instead of in percentage, is the increase larger for silica sol of 0.5 % solid content. But, since the flux are so much higher for 0.5 % is the percentage gained for 5 % greater.

Flux increased with increasing air flow in the air flow interval studied. So it is assumed that the flux could have been higher at greater air flows. The air flow in the tubular membrane increases the hydrodynamic instabilities, which gives a smaller polarization layer. That in turn gives a higher flux over the membrane. (Cheng & Wu, 2003)

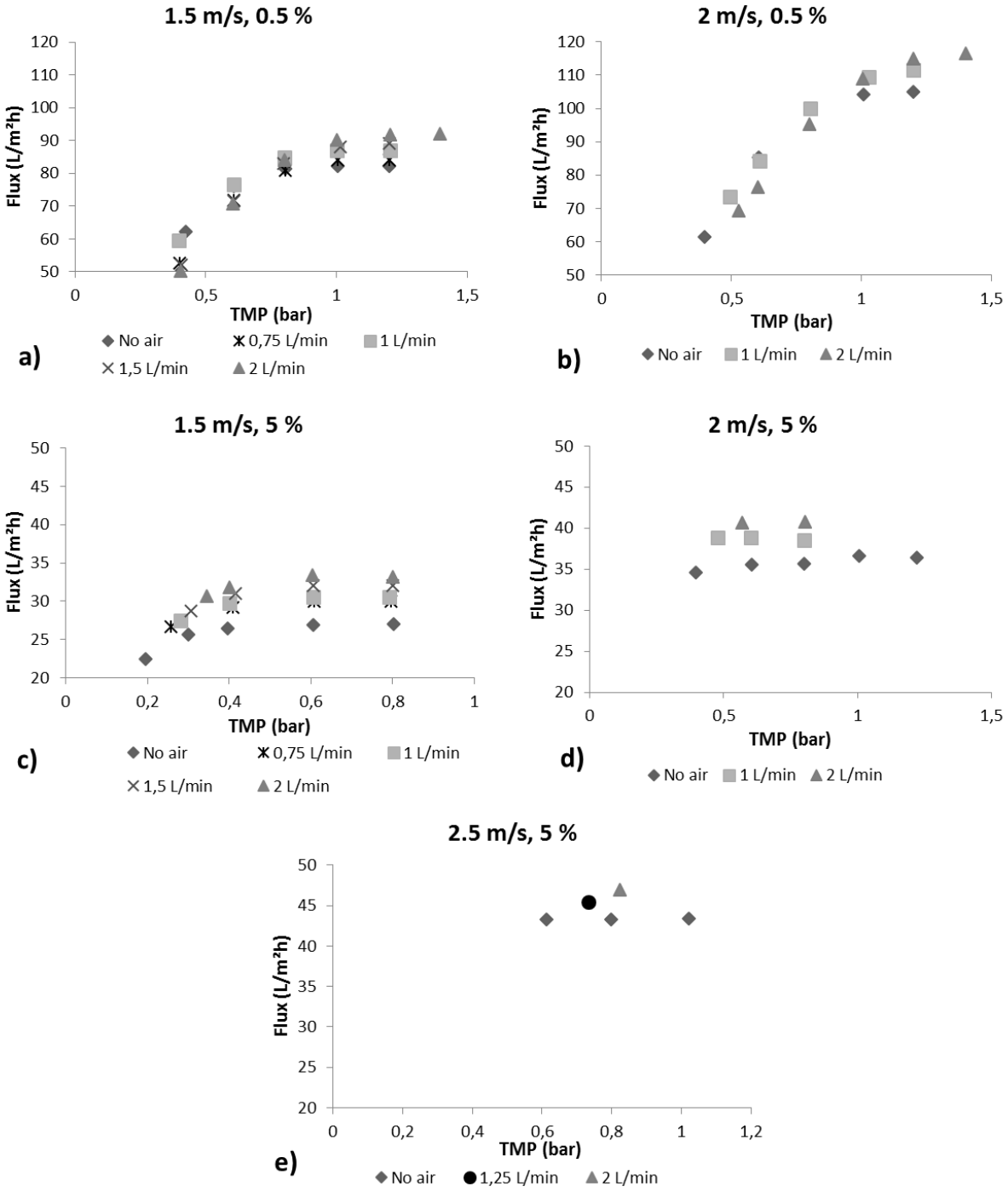

Figure 4.1. Changes in flux depending on TMP and air flow at different liquid flow and silica sol concentrations.

In Table 4.1 is the calculated percentage increase of flux shown. As seen in the table is the increase the largest for higher air flow rate and higher silica sol concentration. For the liquid flow rate 1.5 m/s with a silica concentration of 5 % were the best flux percentage increase of 23 % with the air flow of 2 L/min attained. Since the lowest fluxes were measured under these

condition are it no surprise that the greatest percentage improvement were achieved here, see c) in Figure 4.1.

Table 4.1. The largest percentage increase of flux for the different liquid and air flows.

Liquid flow (m/s)	Air flow (L/min)	0,5 % silica sol	5 % silica sol
1.5	0.75	102.3	110.7
	1	105.8	113.3
	1.5	108.4	118.5
	2	111.9	123.3
2	1	106.2	106.0
	2	110.9	111.5
2.5	1.25	-	104.7
	2	-	108.3

In Figure 4.2 is the air flow plotted against the flux for the different TMPs, liquid flows and silica sol concentrations. It is observed that the flux increase gained from increasing the TMP levels off at one point. The TMP value when this occurs is higher for the lower concentration of silica sol, since the limiting flux is reached later for this concentration.

For 0.5 wt % silica sol is the flux not increasing with higher air flow rate for the lower TMPs, see a) and b) in Figure 4.2. An exact reason for this can not be given, but is believed that it has to do with the type of flow pattern the air and liquid forms. When a transition area between two flow patterns is past through can the flux fluctuate and decrease.

Since the flow patterns during the experiments could not be observed, an option is to consult two-phase flow-pattern maps to find out what they can have been. In the literature, various flow patterns are commonly presented as separate areas with transition boundaries in two-dimensional graphs (Cheng, et al., 2008). The most commonly used axis of these graphs is the liquid and gas superficial velocities. An advantage with these is that it is easy to read the maps with these axes, but a disadvantage is that due to the fact that other variables affect the flow pattern, they are designed for a specific combination of fluids and geometry only. (Abdulmouti, 2014)

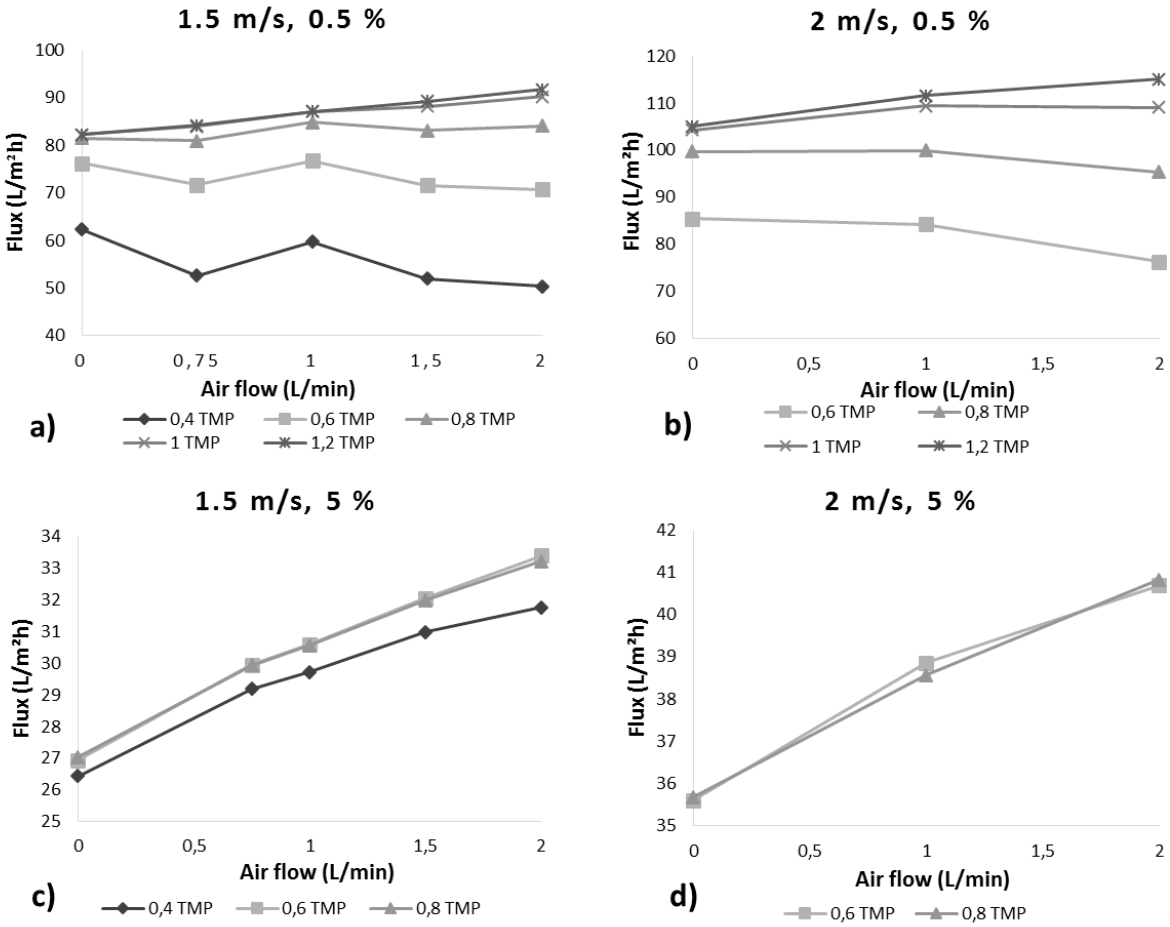

Figure 4.2. Changes in flux depending on air flow and TMP at different flows of liquid and concentration of silica sol.

To find possible flow patterns, three different flow-pattern maps for horizontal pipes have been considered. The first one is the Baker two-phase flow-pattern map for horizontal flow, which is one of the best known empirical flow-pattern maps (Cheng, et al., 2008). It was created from observations of co-current flow of gaseous and condensate petroleum products in horizontal pipes. In the Bakers map is the two parameter groups G_G/λ and $G_L \cdot \psi$ used to determine were on the flow-pattern map the gas-liquid flow are situated. G_G and G_L are the gas and liquid mass velocities. The parameters λ and ψ takes into account the physical properties of the system.

$$\lambda = \left(\frac{\rho_G}{\rho_A} \frac{\rho_L}{\rho_W} \right)^{1/2} \tag{3}$$

Where ρ_G and ρ_L are the densities of gas and liquid at the experiments condition and ρ_A and ρ_W are the densities of air and water at 1 atm pressure and room temperature.

$$\psi = \left(\frac{\sigma_W}{\sigma}\right)\left[\left(\frac{\mu_L}{\mu_W}\right)\left(\frac{\rho_W}{\rho_L}\right)^2\right]^{1/3} \quad (4)$$

Where σ and μ_L are the surface tension and liquid viscosity at the experiments condition and σ_W and μ_W the surface tension and dynamic viscosity of water at 1 atm pressure and room temperature. Calculated values of λ and ψ are found in Appendix A.

The second considered flow-pattern map can be found in (Weisman, et al., 1979) and it is based on experiments with air-water with a 1.2 cm diameter pipe. The parameters used to determine were on the map the gas-liquid flow is situated are the gas and liquid mass flow rates (G_G, G_L). The values of these for the different flow rates are displayed in Appendix A. In the article were it also investigated what would happen to flow-pattern maps if the viscosity were increased. The result from this were that the major flow-patterns had a relatively little change. Another thing was that the transition to homogeneous flow was shifted to lower liquid flows.

The last considered flow-pattern map can be found in (Abdulmouti, 2014) and is the one for air-water with a 1.25 cm diameter pipe. In this one are the gas and liquid volumetric flux (j_G, j_L) used to determine were on the map the gas-liquid flow are situated. A conversion for the air flow from L/min to m/s is shown in Appendix A.

A problem with the flow-pattern maps from Baker and Weisman are that not all values are within the boundary of the maps, due to a low air flow. For Baker are the values for the air flows 0.75 L/min at 0.4-0.8 TMP and 1 L/min at 0.4 TMP either not within or right on the boundary, see Appendix A for all values. The values that are within the boundary are placed in the plug flow field. For the Weisman flow-pattern map is it only the air flows 2 L/min at 0.8-1.2 TMP and 1.5 L/min at 1-1.2 TMP that are within the boundary of the map, see Appendix A for all values. They are placed in a transition region between bubble and plug flow. It can be the transition from bubble to plug flow that makes the flux continue to increase for the higher TMP values.

For the last considered map from Abdulmouti are all values within the boundary of the map. They are situated around the boundary between elongated bubble and disperse flow. It can be this transition area that makes the flux jump up and down in value.

None of these three two-phase flow-pattern maps are generated from experiments with a silica sol liquid. But the ones created with air-water are assumed to be quite close to the truth for the low silica sol concentration of 0.5 %. The Baker flow-pattern map is used because it takes into account the physical properties of the system.

For the silica sol solution with a concentration of 5 % is the flux increase quite linear, see Figures 4.2 c) and d). According to (Weisman, et al., 1979) is the transition to dispersed flow shifted to lower liquid flows for fluids with higher viscosities. This leads to that all values would end up only being on the disperse flow side of the last considered flow-pattern map. Consequently the flux for 5 % silica sol concentration would not be affected of the transition area as 0.5 % concentration can be.

4.2 Experiment with the hemicellulose solution

4.2.1 Flux in experiments

An experiment was performed with fresh alkali extraction solution. Initially, when the retentate flow pipe was below the surface of liquor in the feed tank, was the flux constant at 70 L/m^{2}h. When the pipe was lifted above the surface of the solution in the feed tank, flux increased with time, as shown in Figure 4.3. The flux increase levelled off at 200 L/m^{2}h after about 3 hours after that the retentate flow pipe had been lifted.

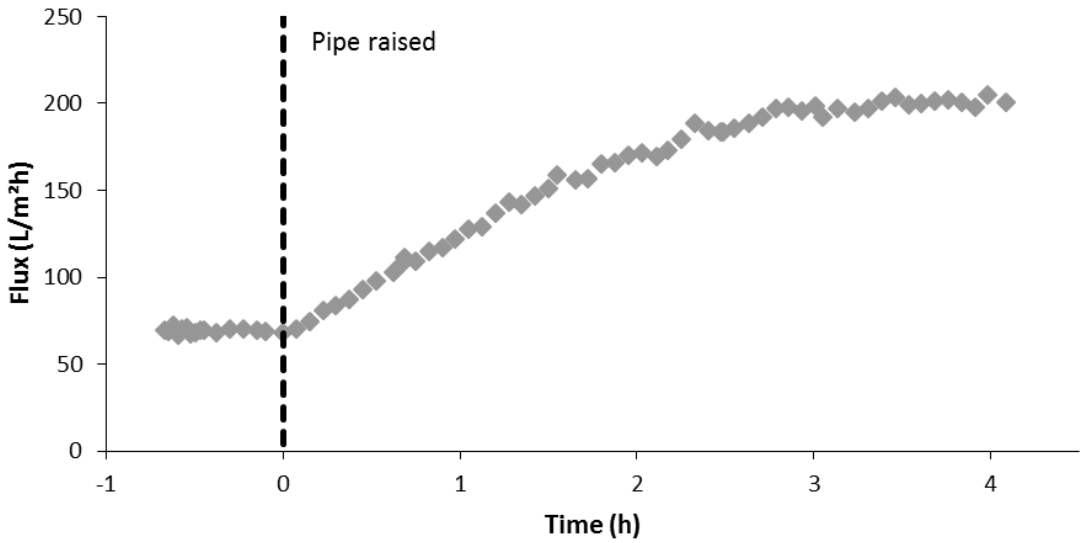

4.3. Flux over time from when the TMP 1.2 bar is reach. The liquid flow is 5 m/s and temperature 80 °C.

The phenomenon shown in Figure 4.3 was also experienced when an older batch of solution was ultrafiltrated. As can be seen in Figure 4.4 a) is almost the same flux increase pattern gotten for the old batch. The difference between them are that the initial flux before the retentate pipe is lifted is 75 L/m^{2}h and the flux levelled off at 190 L/m^{2}h after about 4 hours after that the retentate flow pipe had been lifted for the old batch. Two reasons that can explain why the initial flux were higher for the old batch can be that larger molecules can have started to break down during the storage time or so were it because there was a difference between the two

batches. The lower final flux might also be due to that it was two different batches or so had the molecules in the solution become more stable with time. Since it took longer time before the flux levelled off for the old batch might it very well be that the solution had become more stable during the storage time.

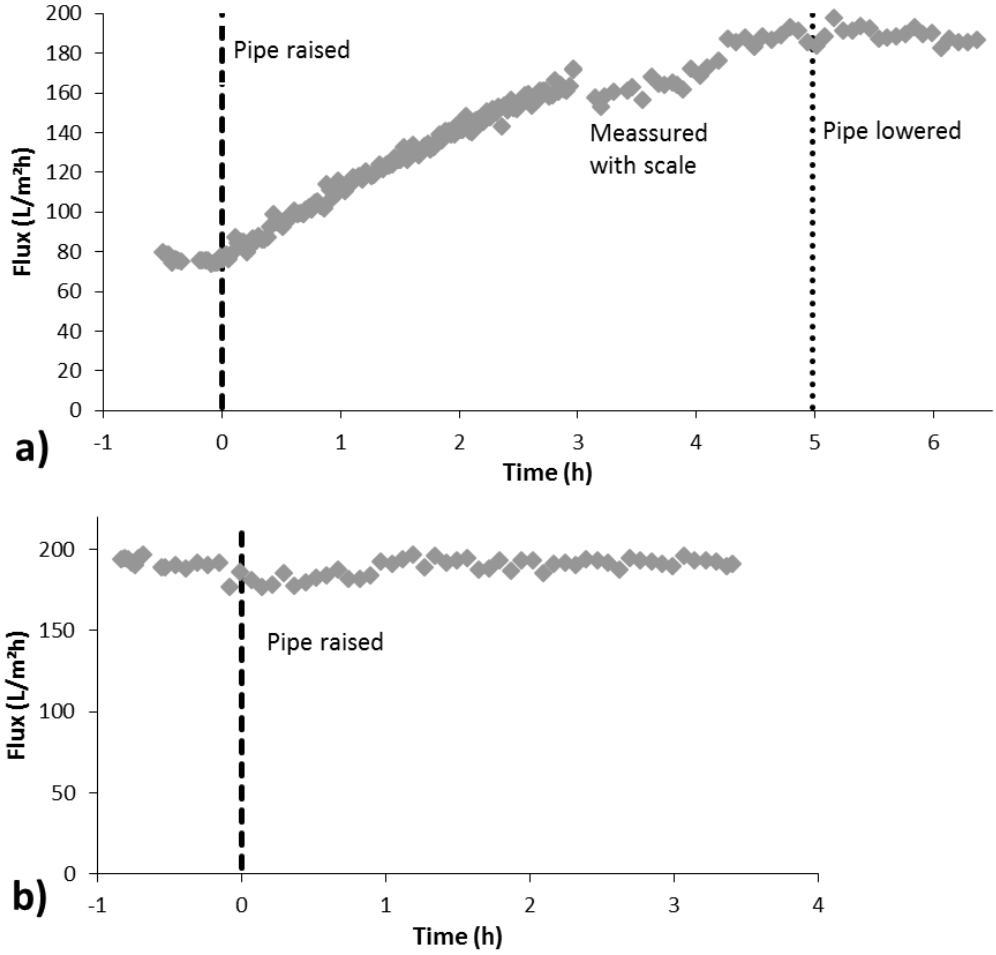

Figure 4.4. Experiments with the old alkali extraction solution. Flux over time from when the TMP 1.2 bar is reach. The liquid flow is 5 m/s and temperature 80 °C. a) First time the solution is used and the retentate pipe is lowered when the flux levelled off. b) Second time the solution is used.

The difference in execution between the two experiments were that when the flux had levelled off for the old solution were the retentate flow pipe lowered under the liquid surface in the feed tank. This were done to see if the flux would decrease when air no longer were whipped into the solution. As can be seen in Figure 4.4 a) did the flux level not decrease, so the experiment were ended and the solution were left in the feed tank over the night. The next day were the same solution run again at 80 °C, to see if the flux had decreased during the night, since the microbubbles should have disappeared from the system during the night. As can be seen in Figure 4.4 b) was that not the case. The flux did not increase when air was whipped down

in the solution. The conclusion drawn from this is that a component is broken down when air is whipped down in the solution in the feed tank. Since the flux increased to a certain level and did not decrease after the air addition were removed.

As shown in Figure 4.5 does the same flux increase not occur when a new experiment were run at the temperature 30 °C. The flux was constant throughout the whole experiment. This indicates that the component that is broken down when experiment is executed at 80 °C needs both heat and air to do so.

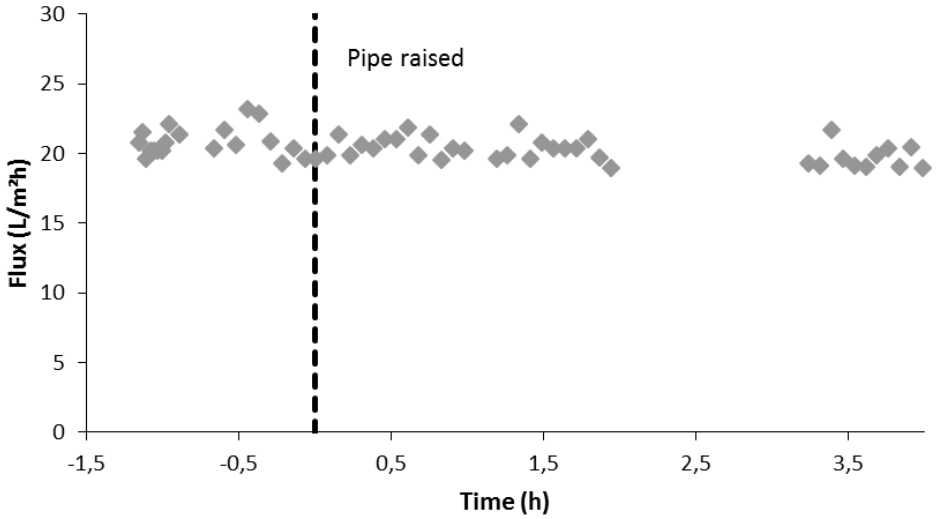

Figure 4.5. Flux over time from when the TMP 1.2 bar is reach. The liquid flow is 5 m/s and temperature 30 °C. Because of air bubbles in the flowmeter no reliable flux values were registered between 2 and 3 hours.

4.2.2 Analysis of solution over time

Samples from feedtank and permeate were withdrawn during the experiments. A remarkable difference between the feed solution used in the experiments was the lower concentration of all parameters but acid-insoluble lignin in the solution used in the 30 °C experiment. The dry solids content was 55 g/l in the 80 °C experiment (see Table 4.2) and 49 g/l in the experiment at 30 °C (see Table 4.3). It is not clear why the concentration was lower in the 30 °C experiment, but it might have something to do with the filtration with kieselguhr. In the experiment at 80 °C two batches of 50 L prefiltered liquor was used whereas one 75 L and a minor amount of one 50 L prefiltered batch was used in the experiment at 30 °C. It is possible that more material was retained in the filter cake when the larger, 75 L volume, was filtered.

Table 4.2. Characteristics of feed (F) and permeate (P) withdrawn at the beginning and at one hour intervals during the experiment at 80 ℃.

Sample	TS [mg/ml]	NaOH [mg/ml]	Arab [mg/g]	Gal [mg/g]	Glu [mg/g]	Xyl [mg/g]	Hemi [mg/g]	Acid-insoluble solids [mg/g]	Acid-soluble lignin [mg/g]	UV abs. (280 nm)
F0	54.66	44.0	1.86	0.25	1.18	4.33	7.62	2.12	0.24	39.6
F1	55.06	44.3	1.94	0.25	1.05	4.35	7.60	2.27	0.27	42.3
F2	53.95	43.9	1.93	0.21	0.97	4.14	7.25	2.02	0.27	42.5
F3	53.41	43.1	1.92	0.21	0.98	4.05	7.15	2.22	0.27	42.1
F4	52.89	42.9	1.83	0.23	0.88	3.89	6.82	2.14	0.28	40.5
P0	44.63	42.4	0.05	0.03	0.13	0.07	0.27	0.56	0.19	25.2
P1	45.08	42.6	0.06	0.03	0.14	0.15	0.38	0.59	0.19	27.3
P2	45.01	42.5	0.06	0.03	0.14	0.15	0.38	0.58	0.18	28.5
P3	45.42	42.2	0.07	0.03	0.15	0.20	0.44	0.64	0.20	29.2
P4	46.09	42.5	0.08	0.03	0.15	0.24	0.50	0.62	0.22	28.9
Av. Ret	16.2%	2.8%	96.7%	86.8%	86.0%	96.1%	94.6%	72.2%	25.8%	32.8%

Table 4.3. Characteristics of feed (F) and permeate (P) withdrawn at the beginning and at one hour intervals during the experiment at 30 ℃.

Sample	TS [mg/ml]	NaOH [mg/ml]	Arab [mg/g]	Gal [mg/g]	Glu [mg/g]	Xyl [mg/g]	Hemi [mg/g]	Acid-insoluble solids [mg/g]	Acid-soluble lignin [mg/g]	UV abs. (280 nm)
F0	49.25	42.0	1.18	0.15	0.59	2.18	4.10	1.82	0.72	37.6
F1	49.37	38.0	1.09	0.16	0.56	2.07	3.88	1.62	0.79	37.7
F2	47.21	38.1	1.10	0.16	0.55	2.06	3.88	1.69	0.72	36.0
F3	50.08	38.4	1.12	0.15	0.57	2.12	3.96	1.69	0.75	38.0
F4	49.77	38.0	1.13	0.14	0.57	2.22	4.05	1.84	0.62	36.6
P0	43.23	36.4	0.03	0.02	0.12	0.04	0.21	0.44	0.15	22.9
P1	42.63	37.1	0.03	0.02	0.12	0.04	0.21	0.40	0.15	23.0
P2	41.58	36.5	0.03	0.02	0.11	0.03	0.19	0.49	0.16	22.3
P3	42.50	37.0	0.03	0.02	0.11	0.03	0.20	0.25	0.14	23.0
P4	42.64	36.9	0.03	0.02	0.12	0.03	0.20	0.53	0.15	23.2
Av. Ret	13.5%	5.4%	97.2%	88.9%	83.8%	98.5%	95.6%	75.6%	79.3%	38.5%

The retention values are similar in the experiments but for the retention of acid-soluble lignin that is 26% in the experiment at 80 °C and 79% at 30 °C. The retention of hemicelluloses was high, about 95%, whereas the retention of NaOH was low, ≤ 5%. Xylose and arabinose had the highest retention and glucse and galactose the lowest retention of sugars. The retention of hemicelluloses decreased with time at 80 °C but was constant at 30 °C, as shown in Figure 4.6. This indicates that the hemicelluloses was degraded during the experiment at 80 °C and hence more hemicelluloses can pass through the membrane. A marked degradation of hemicelluloses with time at 80 °C was also observed by (Arkell, et al., 2013).

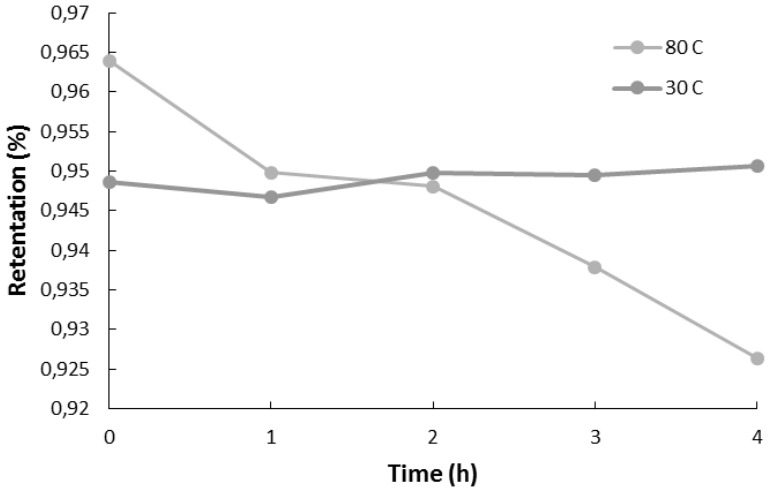

Figure 4.6. Retention of hemicelluloses during ultrafiltration at 80 °C and 30 °C.

Molecular mass distribution of hemicelluloses and lignin

The molecular mass distributions of hemicelluloses and lignin in the retentate and permeate during the experiments were measured for two experiments, one at 80 °C and the other at 30 °C. All the graphs can be seen in Appendix B. For the experiment executed at 30 °C is there no change in either molecular mass of hemicelluloses (expressed in terms of the refractive index) or the molecular mass of lignin (measured as UV absorbance at 280 nm) over time.

For the experiment executed at 80 °C are there changes. The molecular mass of hemicelluloses decreases with time for the solution in the feed tank. That leads to that the amount of hemicelluloses with lower molecular mass increases in the permeate over time, since there are more small hemicelluloses that can pass through the membrane. The molecular mass of lignin decreases with time for the solution in the feed tank too, but to a lesser extent. This distinct that lignin is more stable than the hemicellulose. So there is not much larger lignin to decompose to smaller ones. The amount of lignin with a lower molecular mass is the same in both permeate and feed.

The difference between the two experiments are generally that there are more hemicelluloses and lignin with lower molecular mass for the one executed at 80 °C and more with higher for the one executed at 30 °C. Another difference is that there are four indistinct hemicelluloses peaks for the solution in the feed tank for the 30 °C experiment, but only three in 80 °C. At 80 °C has the hemicelluloses with the highest molecular mass decomposed and filled up the gap between the two peaks with the highest molecular mass.

5 Conclusion

The conclusions drawn from this project are:

- The flux of a silica solution increased when the liquid flow was sparged with air. The flux increase had not levelled off at the highest air flow in the studied air flow interval. So it is assumed that higher fluxes can be obtained with higher air flows than the ones used in this study.
- Limiting flux was reached at the studied TMP intervalls. For the lower silica sol concentration is the limiting flux obtained at 1 bar and for the higher concentration is it at 0.6 bar. The TMP is higher for the lower concentration because the limiting flux is reached later for this concentration.
- The type of flow pattern the two-phase flow forms can greatly affect the flux. In this study the optimal flow pattern were not obtained, since the highest used air flow was too low.
- For the hemicellulose solution a flux increase was obtained if the temperature was 80 °C and air was whipped down in the feed tank. It is believed the reason for the flux increase is that a degradation of molecules that makes more molecules able to pass through the membrane. It was confirmed that a degradation of molecules occurs, but if it was only this that improves the flux can not be verified.
- No increase of flux was observed when the experiment with hemicellulose solution was performed at 30 °C. The molecular degradation that occurs at 80 °C does not arise at 30 °C. That is confirmed by the performed analyses. This indicates that the degradation of molecules only happens at higher temperatures.
- The flux increase obtained when air was whipped down in the feed tank at 80 °C is permanent. This may be caused by a degradation of components in the solution.
- No examination if the arabinoxylan is affected by the heat and addition of air was made. Before the method can by recommended for the industry must this be examined.

6 References

Abdulmouti, H., 2014. Bubbly Two-Phase Flow: Part I- Characteristics, Structures, Behaviors and Flow Patterns. *American Journal of Fluid Dynamics,* 4(4), pp. 194-240.

Antony, A. & Leslie, G., 2011. Degradation of polymeric membranes in water and wastewater treatment. i: *Advanced membrane science and technology for sustainable energy and environmental applications.* u.o.:Woodhead Publishing, pp. 718-745.

Arkell, A., Krawczyk, H. & Jönsson, A.-S., 2013. Influence of heat pretreatment on ultrafiltration of a solution containing hemicelluloses extracted from wheat bran. *Separation and Purification Technology 119,* pp. 46-50.

Bellara, S., Cui, Z. & Pepper, D., 1996. Gas sparging to enhance permeate flux in ultrafiltration using hollow fibre membranes. *Journal of Membrane Science 121,* pp. 175-184.

Cabassud, C., Laborie, S., Durand-Bourlier, L. & Lainé, J., 2001. Air sparging in ultrafiltration hollow fibers: relationship between flux enhancement, cake characteristics and hydrodynamic parameters. *Journal of Membrane Science,* Issue 181, pp. 57-69.

Calabrò, V. & Basile, A., 2011. Fundamental membrane processes, science and engineering. i: *Advanced membrane science and technology for sustainable energy and environmental applications.* u.o.:Woodhead Publishing, pp. 3-21.

Cassano, A. & Basile, A., 2011. Membranes for industrial microfiltration and ultrafiltration. i: *Advanced membrane science and technology for sustainable energy and environmental applications.* u.o.:Woodhead Publishing, pp. 647-679.

Cheng, L., Ribatski, G. & Thome, J. R., 2008. Two-Phase Flow Patterns and Flow-Pattern Maps: Fundamentals and Applications. *Applied Mechanics Reviews,* 61(5), p. 28.

Cheng, T. W. & Wu, J., 2003. Quantitative Flux Analysis of Gas-Liquid Two-Phase Ultrafiltration. i: *Separation Science and Technology, 38:4.* London: Taylor & Francis, pp. 817-835.

Ghajar, A. J., 2005. Non-boiling heat transfer in gas-liquid flow in pipes – a tutorial. *Journal of the Brazilian Society of Mechanical Sciences and Engineering,* 27(1678-5878), pp. 46-73.

Jönsson, A.-S., u.d. *Membranprocesser - Grundläggande begrepp.* Lund: Department for Chemical Engineering, Lunds university.

Krawczyk, H., Arkell, A. & Jönsson, A.-S., 2011. Membrane performance during ultrafiltration of a high-viscosity solution containing hemicelluloses from wheat bran. *Separation and Purification Technology 83,* pp. 144-150.

Krawczyk, H., Arkell, A. & Jönsson, A.-S., 2013. Impact of prefiltration on membrane performance during isolation of hemicelluloses extracted from wheat bran. *Separation and purification Technology 116,* pp. 192-198.

Ralston, J., Fornasiero, D. & Hayes, R., 1999. Bubble–particle attachment and detachment in flotation. *International Journal of Mineral Processing,* 56(1-4), pp. 133-164.

Strathmann, H., 2011. Membranes and Membrane Separation Process, 1. Principles. i: *Ullmann´s Encyclopedia of Industrial Chemestry.* u.o.:u.n.

Thuvander, J., Arkell, A. & Jönsson, A.-S., 2014. Centrifugation as pretreatment before ultrafiltration of hemicelluloses extracted from wheat bran. *Separationand Purification Technology 138,* pp. 1-6.

Weisman, J., Duncan, D., Gibson, J. & Crawford, T., 1979. Effects of fluid properties and pipe diameter on two-phase flow patterns in horizontal lines. *International Journal of Multiphase Flow,* 5(6), pp. 437-462.

Wibisono, Y. o.a., 2013. Two-phase flow in membrane processes: A technology with a future. *Journal of Membrane Science,* pp. 566-602.

Appendix A: Numbers used and calculated for the different flow-pattern maps

Table A.1. Values used for density and viscosity at the different transmembrane pressures (TMP) at 30 °C.

	Density (kg/m^3)		
TMP (bar)	Water	Air	Water viscosity (Pa·s)
0.4	995.6	0.46	0.0008
0.6	995.6	0.69	0.0008
0.8	995.6	0.91	0.0008
1	995.6	1.14	0.0008
1.2	995.6	1.37	0.0008
1 atm	997.2	1.18	0.0009

Table A.2. The surface tension for water at the experiment and standard temperature.

T (°C)	Water surface tension (N/m)
30	0.07116
25	0.07197

Table A.3. The calculated mass flow rate (kg/s) for water and air at their different volume flows and TMP.

TMP	Water (L/min)		Air (L/min)			
(bar)	11.4	15.1	0.75	1	1.5	2
0.4	0.1892	0.2506	$5.750 \cdot 10^{-6}$	$7.667 \cdot 10^{-6}$	$1.150 \cdot 10^{-5}$	$1.533 \cdot 10^{-5}$
0.6	0.1892	0.2506	$8.625 \cdot 10^{-6}$	$1.150 \cdot 10^{-5}$	$1.725 \cdot 10^{-5}$	$2.300 \cdot 10^{-5}$
0.8	0.1892	0.2506	$1.138 \cdot 10^{-5}$	$1.517 \cdot 10^{-5}$	$2.275 \cdot 10^{-5}$	$3.033 \cdot 10^{-5}$
1	0.1892	0.2506	$1.425 \cdot 10^{-5}$	$1.900 \cdot 10^{-5}$	$2.850 \cdot 10^{-5}$	$3.800 \cdot 10^{-5}$
1.2	0.1892	0.2506	$1.713 \cdot 10^{-5}$	$2.283 \cdot 10^{-5}$	$3.425 \cdot 10^{-5}$	$4.567 \cdot 10^{-5}$
1 atm	0.1895	0.2506	$1.475 \cdot 10^{-5}$	$1.967 \cdot 10^{-5}$	$2.950 \cdot 10^{-5}$	$3.933 \cdot 10^{-5}$

Table A.4. The parameters that takes the physical properties of the system into account for the Baker flow-pattern map.

	TMP (bar)				
	0.4	0.6	0.8	1	1.2
λ	0.6238	0.7641	0.8775	0.9821	1.0766
ψ	0.9735	0.9735	0.9735	0.9735	0.9735

Table A.5. The liquid mass velocity and the parameter group $G_L \cdot \psi$ at the different water flows for the Baker flow-pattern map.

Water flow (m/s)	G_L (kg/m^{2}s)	$G_L \cdot \psi$
1.5	1541	1501
2	2042	1988

Table A.6. The gas mass velocity and the parameter group G_g/λ at the different air flows and TMP for the Baker flow-pattern map.

			Air flow (L/min)			
			0.75	1	1.5	2
TMP (bar)	0.4	G_g (kg/m^{2}s)	0.04686	0.06247	0.09371	0.1249
		G_g/λ	0.07510	0.1001	0.1502	0.2003
	0.6	G_g (kg/m^{2}s)	0.07030	0.09371	0.1406	0.1874
		G_g/λ	0.09198	0.1226	0.1840	0.2453
	0.8	G_g (kg/m^{2}s)	0.09269	0.1236	0.1854	0.2472
		G_g/λ	0.1056	0.1408	0.2113	0.2817
	1	G_g (kg/m^{2}s)	0.1161	0.1548	0.2322	0.3097
		G_g/λ	0.1182	0.1576	0.2365	0.3153
	1.2	G_g (kg/m^{2}s)	0.1395	0.1861	0.2404	0.3721
		G_g/λ	0.1296	0.1728	0.2233	0.3456

Table A.7. The liquid mass velocity at the different water flows for the Weisman flow-pattern map.

Water flow (m/s)	G_L (kg/m^{2}h)
1.5	5 549 000
2	7 350 000

Table A.8. The gas mass velocity, G_g (kg/m^{2}h), at the different air volume flows and TMP for the Weisman flow-pattern map.

		Air volume flow (L/min)			
		0.75	1	1.5	2
TMP (bar)	0.4	168.7	224.9	337.4	449.8
	0.6	253	337.4	506	674.7
	0.8	333.7	444.9	667.4	889.8
	1	418	557.4	836.1	1115
	1.2	502.4	669.8	1005	1340

Table A.9. Conversion of air flow from L/min to m/s.

Air flow	
L/min	m/s
0.75	0.0987
1	0.132
1.5	0.1975
2	0.264

Appendix B: Size exclusion chromatograms (SEC)

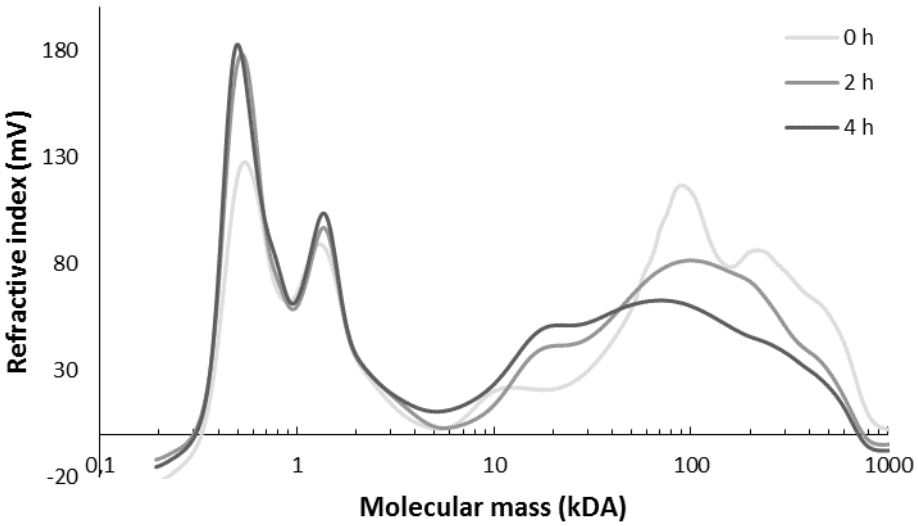

Figure B.1. Refractive index, showing the mass distribution of the hemicelluloses, for the samples taken from the feed tank at the times 0, 2 and 4 h for the experiment carried out at 80 °C with fresh solution.

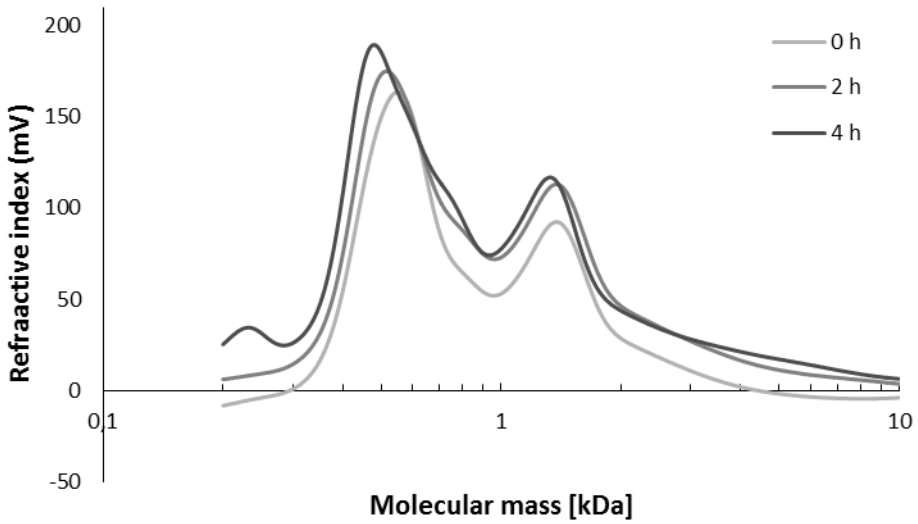

Figure B.2. Refractive index, showing the mass distribution of the hemicelluloses, for the samples taken from permeate at the times 0, 2 and 4 h for the experiment carried out at 80 °C with fresh solution.

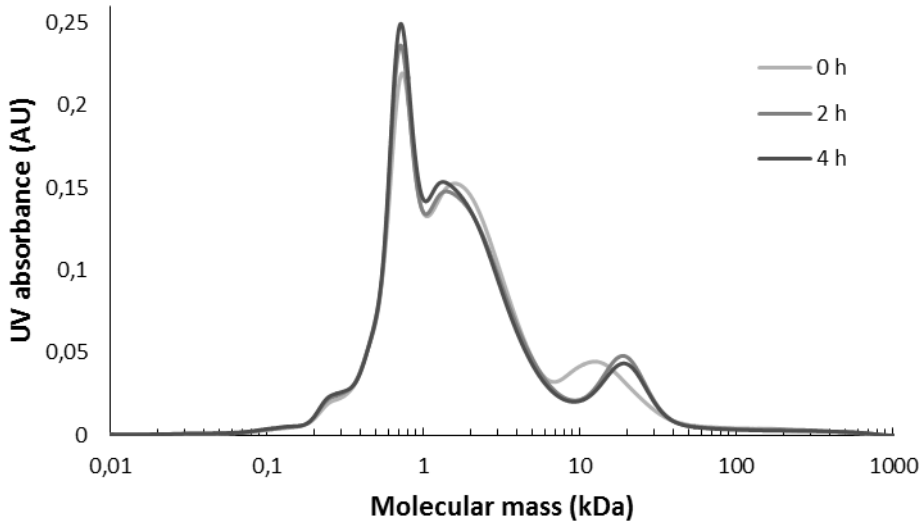

Figure B.3. UV absorption at 280 nm, showing the mass distribution of lignin, for the samples taken from the feed tank at the times 0, 2 and 4 h for the experiment carried out at 80 °C with fresh solution.

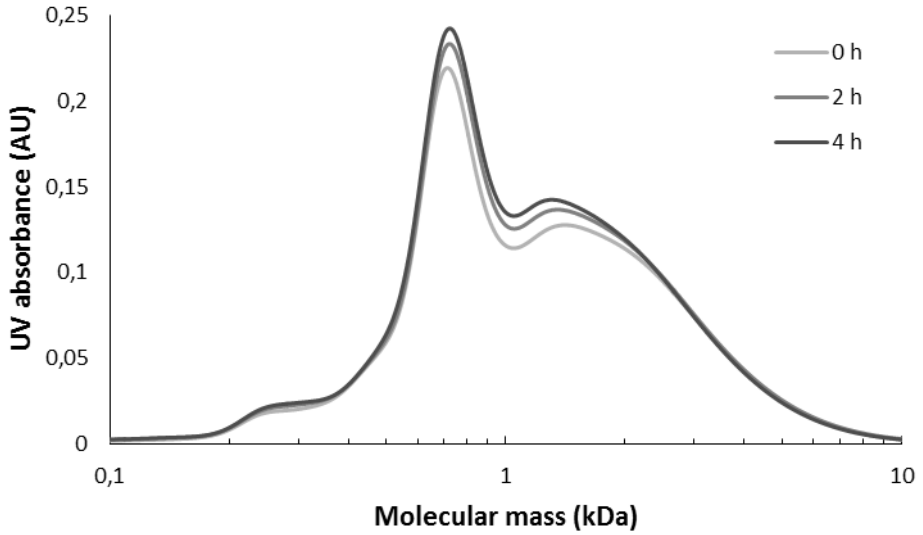

Figure B.4. UV absorption at 280 nm, showing the mass distribution of lignin, for the samples taken from permeate at the times 0, 2 and 4 h for the experiment carried out at 80 °C with fresh solution.

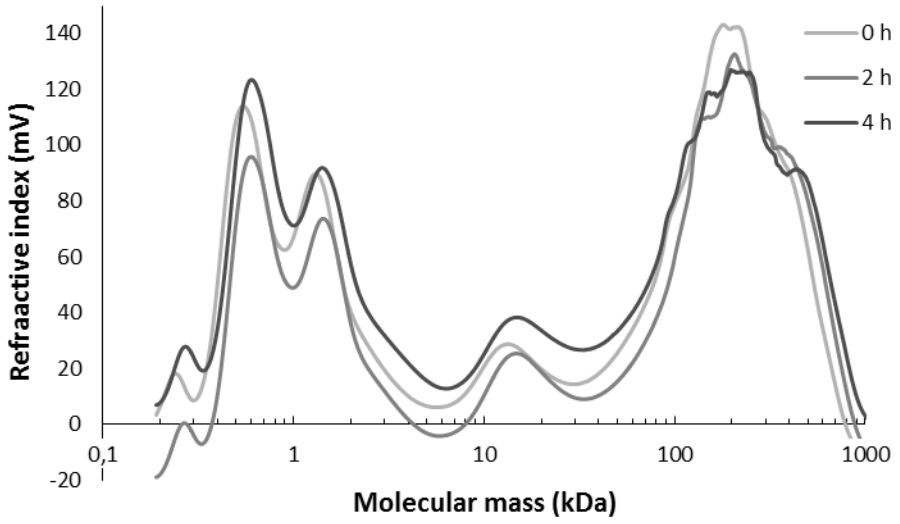

Figure B.5. Refractive index, showing the mass distribution of the hemicelluloses, for the samples taken from the feed tank at the times 0, 2 and 4 h for the experiment carried out at 30 °C with fresh solution.

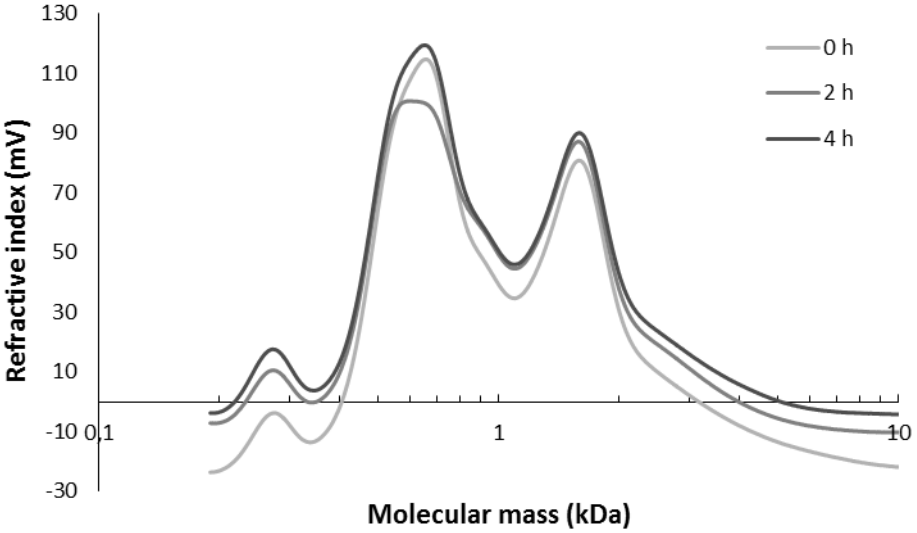

Figure B.6. Refractive index, showing the mass distribution of the hemicelluloses, for the samples taken from permeate at the times 0, 2 and 4 h for the experiment carried out at 30 °C with fresh solution.

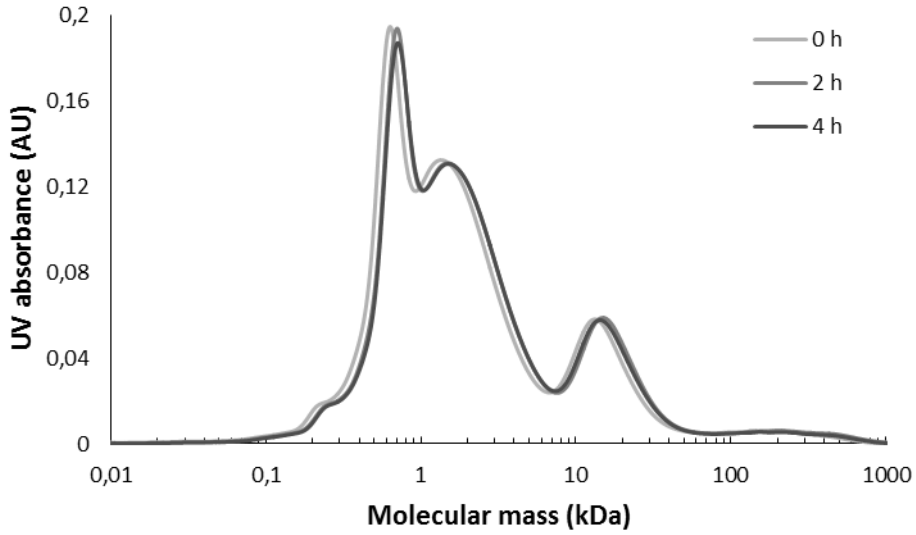

Figure B.7. UV absorption at 280 nm, showing the mass distribution of lignin, for the samples taken from the feed tank at the times 0, 2 and 4 h for the experiment carried out at 30 °C with fresh solution.

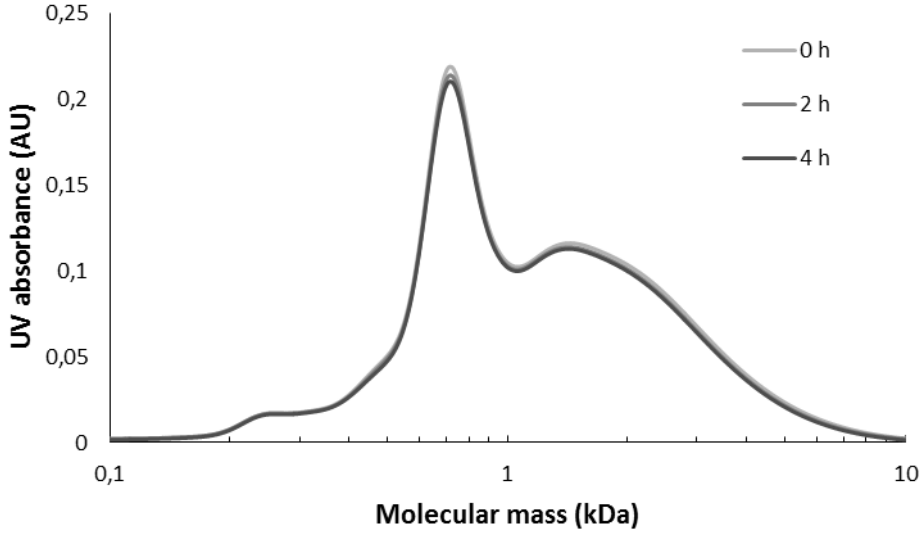

Figure B.8. UV absorption at 280 nm, showing the mass distribution of lignin, for the samples taken from permeate at the times 0, 2 and 4 h for the experiment carried out at 30 °C with fresh solution.